Journal of Photochemistry and Photobiology A: Chemistry 351 (2018) 1–7

Contents lists available at ScienceDirect

Journal of Photochemistry and Photobiology A: Chemistry

journal homepage: www.elsevier.com/locate/jphotochem

A novel colorimetric and fluorescent probe for trivalent cations based on rhodamine B derivative

Xiao-li Yue, Chao-rui Li, Zheng-yin Yang*

College of Chemistry and Chemical Engineering, State Key Laboratory of Applied Organic Chemistry, Lanzhou University, Lanzhou 730000, PR China

ARTICLE INFO

Article history:
Received 7 August 2017
Received in revised form 2 October 2017
Accepted 3 October 2017
Available online 5 October 2017

Keywords:
Fluorescent probe
Colorimetric
Rhodamine B
Ring-open
Trivalent cations
Reversibility

ABSTRACT

A novel Schiff-base **(HL)** based on rhodamine B derivative was designed and synthesized as a highly selective and sensitive "turn-on" fluorescent probe for M^{3+} (Cr^{3+}, Fe^{3+}, and Al^{3+}) in methanol. Upon addition of M^{3+}, the spirolactam ring (colorless and nonfluorescent) of **HL** was opened to the ring-open forms (pink and orange-yellow fluorescence). These results indicated that **HL** could be used as a colorimetric and fluorescent probe for the detection of M^{3+} with low detection limit of 0.63 μM (Cr^{3+}), 0.14 μM (Fe^{3+}), and 0.22 μM (Al^{3+}). The binding constant (Ka) of M^{3+} binding to **HL** were calculated to be $0.87 \times 10^4\ M^{-1}$ (Cr^{3+}), $1.14 \times 10^4\ M^{-1}$ (Fe^{3+}), and $4.48 \times 10^4\ M^{-1}$ (Al^{3+}), respectively from a Benesi-Hildebrand plot. The binding stoichiometry between **HL** and M^{3+} was determined from the Job's plot (fluorescent spectrum) and ESI–MS spectrum data to be 1:1. Furthermore, the recognition process of the probe for M^{3+} was chemically reversible on the addition of fluorinion (F^-).

1. Introduction

The design and synthesis of new chemosensors for trivalent metal ions (M^{3+}) is an important research subject because of their biological significance and environmental importance. For instance, as the third most abundant metal in the Earth's crust, aluminum is widely used in aluminum alloy, aircraft, automobiles, trains, ships and other manufacturing industries [1–8]. However, overdose of Al^{3+} not only disturbs Ca^{2+} metabolism, decreases liver and kidney function, but also causes Alzheimer's disease and osteoporosis [9–12]. Cr^{3+}, an essential trace element in human nutrition, affects the metabolism of carbohydrates, fats, proteins and nucleic acids through activating certain enzymes and stabilizing proteins and nucleic acids. Excessive Cr^{3+} has a negative impact on cellular structure, cellular function, glucose levels, and lipid metabolism, while deficient Cr^{3+} may cause diabetes and cardiovascular disease [13,14]. Moreover, industrial runoff of Cr^{3+} may cause adverse impact on industry and agriculture [15,16]. Fe^{3+}, an essential trace element in biological systems, plays an important role in many chemical and biological processes such as electron transfer reactions and oxygen transport due to its adequate redox potentials and high affinity for oxygen [17,18]. Overdose of Fe^{3+} may cause some dysfunction of heart, pancreas, and liver, while the deficiency of Fe^{3+} may also cause anemia, hemochromatosis, liver damage, diabetes, and Parkinson's disease [19–22]. Therefore, it's significant to design and synthesize optical chemosensors for detecting the presence of trivalent cation ions (Cr^{3+}, Fe^{3+}, and Al^{3+}) in environmental and biological samples.

Over the past few years, a large number of chemosensors for trivalent metal ions (Cr^{3+}, Fe^{3+}, and Al^{3+}) have been reported [23–28]. Barba-Bon et al. described a highly selective fluorescent probe for trivalent cation ions (Cr^{3+}, Fe^{3+}, and Al^{3+}) based on derivative of fluorescein [11]. Recently, Samanta also reported a new fluorogenic probe for sensing of trivalent cations in live cells [28]. However, the two probes may face some challenges in bioimaging application due to indigo fluorescence (475 nm) [11] and green fluorescence (509 nm) [28]. In vivo fluorescence tracking studies, emission at longer wavelengths is satisfactory because of the improved photon tissue penetration and reduced background autofluorescence, especially emission in the NIR region [29–32]. Tang et al. developed a fluorescent probe emitting red fluorescence for detecting trivalent cations [12]. However, the probe had poor selectivity for trivalent cations because it also responded towards Hg^{2+} in similar condition.

The rhodamine B derivatives are excellent fluorophores due to large molar extinction coefficient, high fluorescence quantum yield, and long absorption, emission wavelengths. On the basis of the equilibrium between spirocyclic (non-fluorescent) and ring-open forms (highly fluorescent) [33–35], we designed and synthesized a new turn-on fluorescent probe for the detection of trivalent cations. The rhodamine B skeleton was used as the

* Corresponding author.
E-mail address: yangzy@lzu.edu.cn (Z.-y. Yang).

https://doi.org/10.1016/j.jphotochem.2017.10.005
1010-6030/

fluorophore and chromophore and the (4-Hydroxybenzoyl)hydrazine was used as the recognition group. The introduce of a hydroxyl group in the terminal benzene ring could strengthen the electron cloud density of the *para*-position (C=O) to enhance the oxygen coordination ability. The probe, 2-[[3′,6′-bis(diethylamino)-3-oxospiro[1-isoindoline-1,9′-xanthen]-2-yl]imino]acetaldehyde-(4-hydroxybenzoyl)hydrazone **(HL)** exhibited high selectivity towards trivalent cations over commonly monovalent and divalent metal ions in methanol. Significantly, the binding of **HL** and trivalent cations was chemically reversible by the addition of F^- solution.

2. Experimental section

2.1. Materials and instruments

Rhodamine B and cationic salts such as $Al(NO_3)_3$, $Ba(OAc)_2$, $Ca(NO_3)_2$, $Cd(OAc)_2$, $Co(OAc)_2$, $Cr(NO_3)_3$, $Cu(NO_3)_2$, $Fe(NO_3)_2$, $Fe(NO_3)_3$, K(OAc), $Mg(NO_3)_2$, $Mn(NO_3)_2$, $NaClO_4$, $Ni(NO_3)_2$, Pb $(OAc)_2$, $Zn(NO_3)_2$, $Li(NO_3)$, $Ag(NO_3)$, and $HgCl_2$ were obtained from commercial suppliers and used without further purification. ^{1}H NMR spectrum were measured on the JNM-ECS 400 MHz spectrometer. Chemical shifts are reported in ppm using TMS as an internal standard. ESI–MS were determined on a Bruker esquire 6000 spectrometer. UV–vis absorption spectrum were measured with a Shimadzu UV-240 spectrophotometer. Fluorescence spectrum were determined on a Hitachi RF-4500 spectrophotometer equipped with quartz cuvettes of 1 cm path length. The melting point was determined on a Beijing XT4–100 x microscopic melting point apparatus.

2.2. Synthesis

(4-Hydroxybenzoyl)hydrazine was synthesized according to the method reported [36]. The **HL** was synthesized according to the route as shown in Scheme 1.

2.2.1. Synthesis of rhodamine B hydrazine (1)

To a 0.8 g of rhodamine B dissolved in 30 mL of methanol, an excessive hydrazine hydrate (1 mL) was added and then the reaction solution was refluxed till the pink color disappeared. After cooling to room temperature, the solvent was removed under reduced pressure. The precipitate was washed with deionized water and dried under reduced pressure to give the final product in the field of 64%. Melting point: 192–195 °C. ^{1}H NMR (400 MHz, $CDCl_3$, TMS) (Fig. S1): δ_H ppm 1.16 (t, 12H, NCH_2CH_3, J = 6.8 Hz), 3.33 (q, 8H, NCH_2CH_3, J = 6.8 Hz), 3.60 (s, 2H, N—NH_2), 6.28 (m, 2H), 6.41-6.46 (m, 4H), 7.09-7.11 (m, 1H), 7.44 (m, 2H), 7.92 (m, 1H). ^{13}C NMR (400 MHz, $CDCl_3$, TMS) (Fig. S2): δ_C ppm 12.63 (CH_3), 44.88 (CH_2), 66.33, 98.08, 104.67, 108.12, 122.95, 124.24, 128.17, 130.35, 133.00, 149.12, 151.65, 154.33, 166.53 (C=O).

2.2.2. Synthesis of 2-[[3′,6′-bis(diethylamino)-3-oxospiro[1-isoindole-1,9′-xanthe-n]-2-yl]imino]acetaldehyde (2)

Rhodamine B hydrazine (0.46 g) was dissolved in absolute ethanol (30 mL). An excess of glyoxal (2 mL) was added, and the mixture was stirred overnight at room temperature. Then plenty of saturated potassium chloride solution was added to precipitate the crude product. The crude product was collected, washed with ethanol and water, and dried under reduced pressure. ^{1}H NMR (400 MHz, $CDCl_3$, TMS) (Fig. S3): δ_H ppm 1.16 (t, 12H, NCH_2CH_3, J = 6.4 Hz), 3.33 (q, 8H, NCH_2CH_3, J = 6.4 Hz), 6.25 (d, 2H, Ar-H, J = 8.4 Hz), 6.40-6.46 (m, 4H, Ar-H), 7.10 (d, 1H, Ar-H, J = 7.6 Hz), 7.38 (d, 1H, CH=N, J = 7.2 Hz), 7.46-7.56 (m, 2H, Ar-H), 8.04 (d, 1H, Ar-H, J = 7.2 Hz), 9.44 (d, 1H, CH=O, J = 7.6 Hz). ^{13}C NMR (400 MHz, $CDCl_3$, TMS) (Fig. S4): δ_C ppm 12.69 (CH_3), 44.45 (CH_2), 66.05, 98.17, 103.79, 108.27, 123.95, 124.14, 126.72, 127.82, 128.82, 134.74, 141.21, 149.32, 152.66, 153.04, 166.04 (C=O), 192.71 (CHO).

2.2.3. Synthesis of 2-[[3′,6′-bis(diethylamino)-3-oxospiro[1-isoindole-1,9′-xanthe-n]-2-yl]imino]acetaldehyde-(4-hydroxybenzoyl) hydrazone 3 (HL)

2-[[3′,6′-bis(diethylamino)-3-oxospiro[1-isoindole-1,9′-xanthen]-2-yl]imino]acetaldehyde (0.2483 g, 0.5 mmol) and (4-hydroxybenzoyl)hydrazine (0.0761 g, 0.5 mmol) were mixed in 40 mL ethanol and refluxed overnight under N_2. After cooling to room temperature, the precipitate was collected, washed with cold ethanol, and dried in vacuum. Yields: 40%. Melting point: 218 °C. ^{1}H NMR (400 MHz, DMSO-d_6, TMS) (Fig. S5): δ_H ppm 11.68 (s, 1H), 10.17 (s, 1H), 7.98 (s, 1H), 7.92 (d, 1H, J = 7.6 Hz), 7.85 (s, 1H), 7.79 (d, 1H, J = 8.8 Hz), 7.70 (d, 2H, J = 8.8 Hz), 7.60 (t, 1H, J = 7.6 Hz), 7.55 (t, 1H, J = 7.6 Hz), 7.06 (d, 1H, J = 7.6 Hz), 6.85 (dd, 2H, J = 8.8 Hz, J = 16.8 Hz), 6.45 (d, 1H, J = 2 Hz), 6.43 (s, 1H), 6.41 (s, 1H), 6.37 (d, 1H, J = 2.4 Hz), 6.35 (d, 1H, J = 2.4 Hz), 3.36-3.29 (q, 8H), 1.09 (t, 12H, J = 6.8 Hz). ^{13}C NMR (400 MHz, DMSO-d_6, TMS) (Fig. S6): δ_C ppm 30.36 (CH_3), 55.35 (CH_2), 98.44, 106.99, 112.50, 119.03, 119.35,

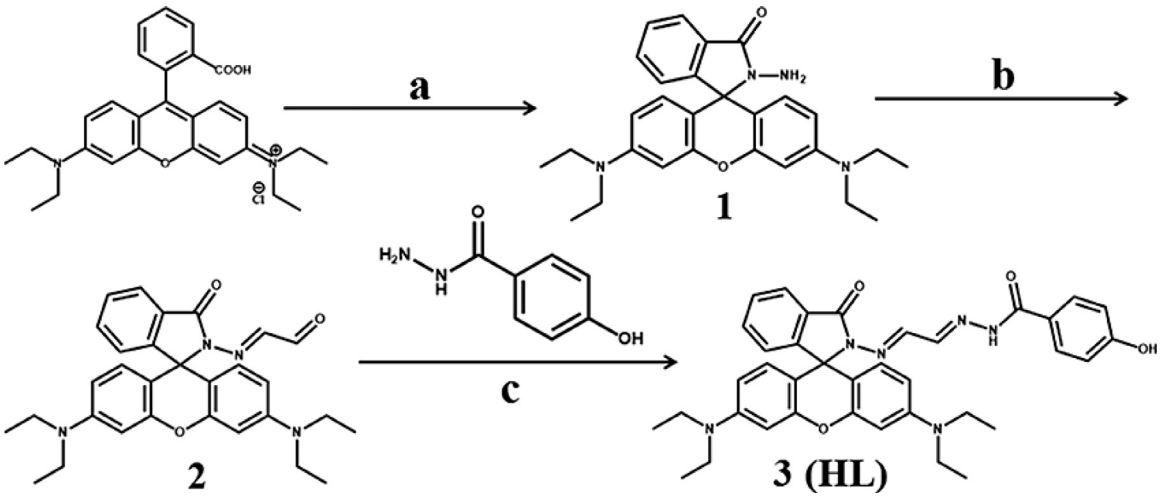

Scheme 1. The synthetic route of 2-[[3′,6′-bis(diethylamino)-3-oxospiro[1-isoindole-1,9′-xanthen]-2-yl]imino]acetaldehyde-(4-hydroxybenzoyl)hydrazone **(HL)**. Reagents and conditions: (a) methanol, hydrazine hydrate, 65 °C, reflux, 12 h, compound 1 Yields: 64%; (b) absolute ethanol, glyoxal, saturated potassium chloride solution, room temperature, 24 h, compound 2 Yields: 72%; (c) absolute ethanol, 80 °C, reflux, 24 h, compound 3 Yields: 40%.

122.28, 123.46, 124.28, 127.95 (3 °C), 103.96, 119.07, 119.18, 122.13, 139.35, 142.11, 149.20, 151.81 (4 °C). ESI–MS (Fig. S7) calculated for $[M+H]^+$ 631.7452, found 631.3431.

2.3. UV-vis and fluorescence spectra measurements

Stock solutions of 5×10^{-3} M various metal ions and **HL** were prepared in ethanol and DMF, respectively. Additionally, the stock solution of NaF was also prepared in distilled water. All absorption and emission spectrum were performed in a quartz optical cell of 1 cm optical path length at room temperature. All fluorescence measurements were carried out upon excitation at 480 nm, and the emission was recorded from 500 to 700 nm. Both excitation and emission slit widths were 3 nm.

3. Results and discussion

The fluorescent emission of **HL** (50 μM) towards trivalent cations showed an excitation-independent feature due to the relative uniform surface state and size distribution [37,38]. As the excitation wavelength varied from 360 to 480 nm (Fig. S8), their maximum emission was all located at 583 nm, the strongest emission intensity was obtained when the excitation wavelength was fixed at 480 nm. Fig. S9 demonstrated fluorescent emission data in different solvents. It could be seen in Fig. S9 that the emission maximum was observed in methanol. To find out the effect of water content in the fluorogenic response of **HL** towards trivalent cations, we recorded the emission changes of **HL** towards M^{3+} in different fractions of water-methanol mixture and the strongest emission was obtained in absolute methanol (Fig. S10). Therefore, further UV/vis and fluorescent studies were carried out in absolute methanol.

3.1. UV/vis studies of HL towards M^{3+}

The UV/vis spectrum of **HL** (50 μM) towards various metal ions (Li^+, Na^+, K^+, Ag^+, Ca^{2+}, Mg^{2+}, Ba^{2+}, Zn^{2+}, Cu^{2+}, Fe^{2+}, Ni^{2+}, Cd^{2+}, Co^{2+}, Pb^{2+}, Mn^{2+}, Hg^{2+}, Cr^{3+}, Fe^{3+}, and Al^{3+}) was illustrated in Fig. 1. As shown in Fig. 1, the solution of **HL** in methanol was colorless and exhibited no absorption at 558 nm in the absence of M^{3+} due to the spirolactam form of **HL**. Upon addition of M^{3+} (Cr^{3+}, Fe^{3+}, and Al^{3+}), a new and strong absorption peak at 558 nm appeared with the solution color changing from colorless to pink, which was attributed to the formation of the strongly fluorescent ring-opened **HL**-M^{3+} complex. Such a dramatic color change suggested that **HL** could serve as a "turn-on" and colorimetric fluorescent probe for M^{3+}. Other monovalent and divalent cations did not show

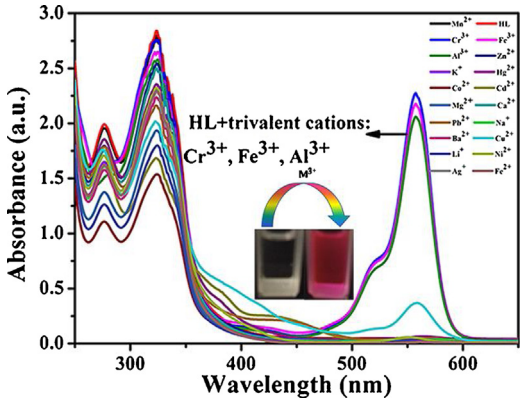

Fig. 1. UV-vis spectrum of **HL** (50 μM) before and after of *1 equiv. of* various metal cations in methanol. (inset) Visible color change of **HL** upon addition of M^{3+} in ambient light.

any significant color and spectral changes under the identical conditions, except for Cu^{2+}, which resulted in a slight change of absorbance at 558 nm. Whereas, when the solution containing **HL** and Cu^{2+} was subjected to fluorescence, the solution showed no fluorescence (Fig. 3) due to the paramagnetic nature [39–41].

In addition, the absorption titrations of **HL** (50 μM) towards M^{3+} in methanol were carried out (Fig. 2). Upon addition of M^{3+} (0–100 μM), the absorbance band at 558 nm gradually increased with the increase of M^{3+} concentration. Simultaneously, the absorbance bands (262 and 293 nm for Cr^{3+}, 266 and 290 nm for Fe^{3+}, 265 and 292 nm for Al^{3+}) increased, while the bands (278 and 323 nm for Cr^{3+}, 277 and 322 nm for Fe^{3+}, 277 and 325 nm for Al^{3+}) decreased. These results clearly illustrated the process of M^{3+} metal ions-induced the ring opening of the spirolactam.

3.2. Fluorescence studies of HL towards M^{3+}

The emission of **HL** (50 μM) towards various metal ions (Li^+, Na^+, K^+, Ag^+, Ca^{2+}, Mg^{2+}, Ba^{2+}, Zn^{2+}, Cu^{2+}, Fe^{2+}, Ni^{2+}, Cd^{2+}, Co^{2+}, Pb^{2+}, Mn^{2+}, Hg^{2+}, Cr^{3+}, Fe^{3+}, and Al^{3+}) was shown in Fig. 3. **HL** alone did not exhibited any fluorescent emission in methanol, which suggested that **HL** still existed in spirolactam form. Upon addition of M^{3+}, a new and strong emission band at 583 nm (orange-yellow fluorescence) was observed, which indicated that M^{3+} induced the ring-open formation of **HL**. However, other monovalent and divalent cations did not cause any significant changes under the same conditions. These results indicated that **HL** had high selectivity towards M^{3+} over other monovalent and divalent cations.

To obtain more insight into the fluorescent properties of **HL** as a chemosensor for M^{3+}, fluorescent titration experiments of **HL** (50 μM) towards increasing amounts of M^{3+} (0–100 μM) were carried out (Fig. 4). As shown in Fig. 4, **HL** hardly exhibited fluorescent emission at 583 nm below 20 μM because the binding between M^{3+} and the nitrogen atom in the spirolactam did not induce successively the ring-open of rhodamine B. Upon addition of above 20 μM M^{3+} to **HL** solution (50 μM), the spirolactam was opened along with the appearance of fluorescent emission peak at 583 nm and the fluorescence intensity at 583 nm was gradually increased with the progressive addition of M^{3+} and the intensity remained constant after the addition of 2 equivalent of M^{3+} (Cr^{3+}, Fe^{3+}, and Al^{3+}). These results suggested that **HL** could detect M^{3+} quantitatively with a large range.

3.3. Interference studies from other valent metal ions

As we all know, an ability to resist interference from other analytes is an important characterization for a chemosensor. The competitive experiments of **HL** (50 μM) towards M^{3+} in the presence of other valent cations (Li^+, Na^+, K^+, Ag^+, Ca^{2+}, Mg^{2+}, Ba^{2+}, Zn^{2+}, Cu^{2+}, Fe^{2+}, Ni^{2+}, Cd^{2+}, Co^{2+}, Pb^{2+}, Mn^{2+}, Hg^{2+}) were conducted (Fig. 5). It was noticeable that the competitive metal ions did not cause any significant changes in the fluorescence intensities of **HL**-M^{3+} (except Hg^{2+} and Mn^{2+}). This experimental results indicated that monovalent and divalent cations did not influence the fluorogenic response of **HL** towards M^{3+}. Therefore, **HL** could be used as a highly selective fluorescent probe for M^{3+}.

3.4. Reversible test of HL towards M^{3+} by NaF

Reversibility and regeneration are important indexes in practical applications for a chemosensor. To examine the reversibility of the **HL**-M^{3+} complex, 2 equivalent NaF was added to **HL**-M^{3+} solutions. As shown in Fig. 6, upon addition of 2 equivalent NaF to the solutions of **HL**-M^{3+} complex, the solution color changed from pink to colorless and the fluorescence intensity

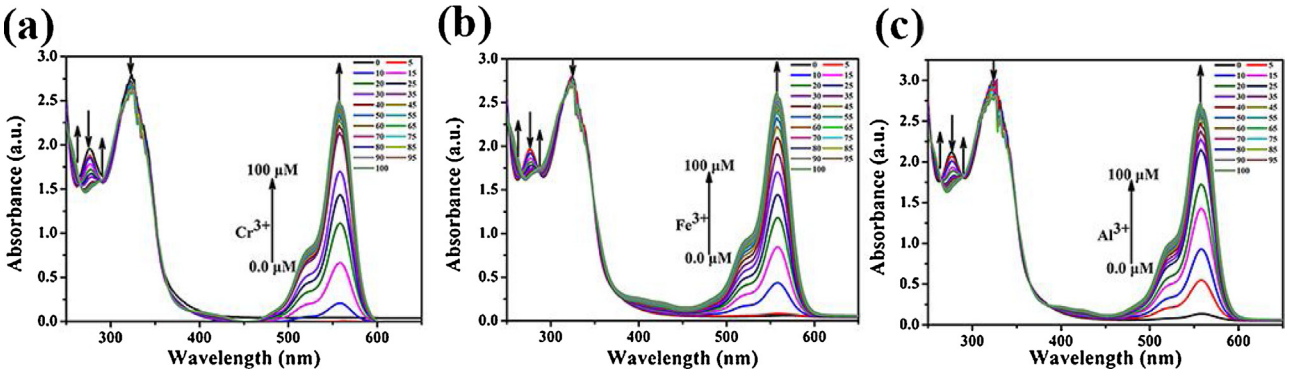

Fig. 2. UV-vis spectrum of **HL** (50 μM) in the presence of M^{3+} (0–100 μM) in methanol. (a): Cr^{3+}, (b): Fe^{3+}, and (c): Al^{3+}.

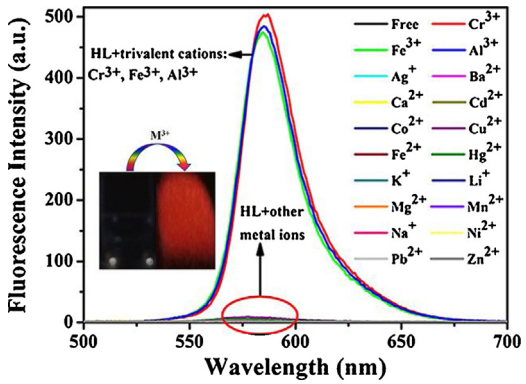

Fig. 3. Fluorescence emission spectrum of **HL** (50 μM) before and after of *1 equiv. of* various metal ions in methanol. (inset) Fluorescence emission color change of **HL** upon addition of M^{3+} after illumination under UV light.

of the system was quenched obviously, demonstrating that M^{3+} was captured from **HL**-M^{3+} by NaF accompanied with the regeneration of the free **HL** due to the binding constant of M^{3+} with F^- is larger than that with **HL**. Then the M^{3+} was again added to the system, the solution color changed from colorless to pink and the fluorescence signals of the system were partly recovered. These results suggested that **HL** is a chemically reversible fluorescent probe for M^{3+}.

This type of reversible behavior of **HL** mimics the INHIBIT logic gate (integrated by combining a NOT, a YES, and an AND gate). The INHIBIT logic gate, the truth table, and the output signals of fluorescence are shown in Fig. 7. In this logic gate, M^{3+} and F^- are used as input1 and input2 respectively. We define the presence of analytes as a "1" state and the absence of analytes as a "0" state. When input1 and input2 are "0" state, the output is "0" state (no fluorescence). When upon addition of F^- to **HL** solution (50 μM), *i.e.* input1 is "0" state and input2 is "1" state, the output is "0" state (no fluorescence). When we add M^{3+} to **HL** solution (50 μM), *i.e.* input1 is "1" state and input2 is "0" state, the output is "1" state (strong fluorescence). When upon addition of F^- to **HL**-M^{3+} solution, *i.e.* input1 is "1" state and input2 is "1" state, the output is "0" state (no fluorescence).

3.5. Binding constant, stoichiometry and detection limit

Association constant (Ka) and detection limit (LOD) of **HL** for M^{3+} (Cr^{3+}, Fe^{3+}, and Al^{3+}) were obtained from the fluorescence titration experiments. The association constant (Ka) of **HL**-M^{3+} complex was determined by the Benesi-Hildebrand equation [42]: $\frac{1}{F-F_{min}} = \frac{1}{K(F_{max}-F_{min})[M^{3+}]} + \frac{1}{F_{max}-F_{min}}$ where F is the fluorescence intensity at 583 nm at any given M^{3+} concentration, F_{min} is the fluorescence intensity at 583 nm in the absence of M^{3+}, and F_{max} is the maximal fluorescence intensity at 583 nm in the presence of M^{3+}. The Ka values of **HL**-M^{3+} complex were calculated to be $0.87 \times 10^4\ M^{-1}$ (Cr^{3+}), $1.14 \times 10^4\ M^{-1}$ (Fe^{3+}), and $4.48 \times 10^4\ M^{-1}$ (Al^{3+}), respectively by the plotting $1/(F\text{-}F_{min})$ against $1/[M^{3+}]$ (Fig. S11) according to the Benesi-Hildebrand equation. The detection limit (LOD) of **HL** for M^{3+} were calculated to be 0.63 μM (Cr^{3+}), 0.14 μM (Fe^{3+}), and 0.22 μM (Al^{3+}) according to the equation: $DL = 3\sigma/K$ where σ is the standard deviation of the blank solution and K is the slope of the calibration curve (Fig. S12, Fig. S13, and Fig. S14) from the fluorescence titration experiments [43]. The binding stoichiometry of **HL** towards M^{3+} was obtained from the Job's method on the basis of fluorescence emission spectrum. As shown in Fig. 8, the emission intensity showed a maximum when the molar fraction of

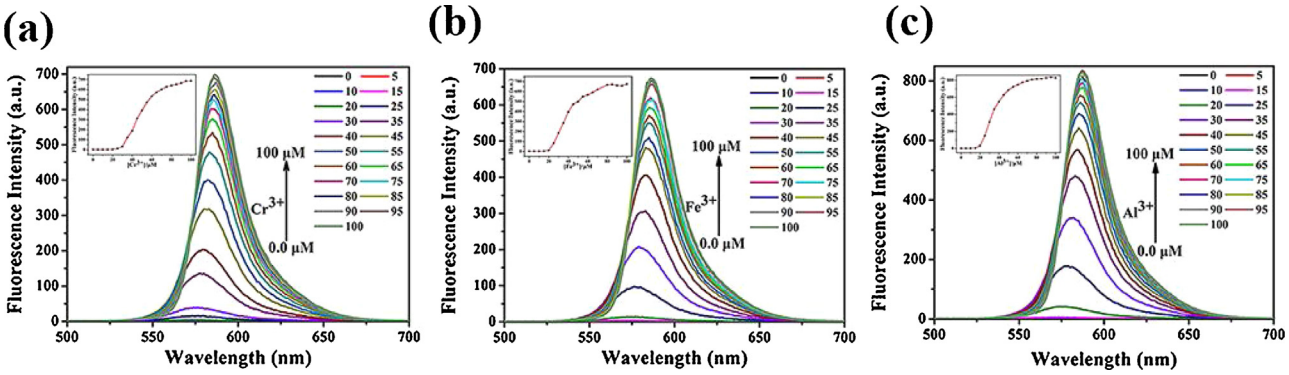

Fig. 4. Fluorescence emission spectrum of **HL** (50 μM) in the presence of M^{3+} (0–100 μM) in methanol. (a): Cr^{3+}, (b): Fe^{3+}, and (c): Al^{3+}. Inset: Changes of fluorescence intensity of **HL** at 583 nm upon the addition of progressive $[M^{3+}]$.

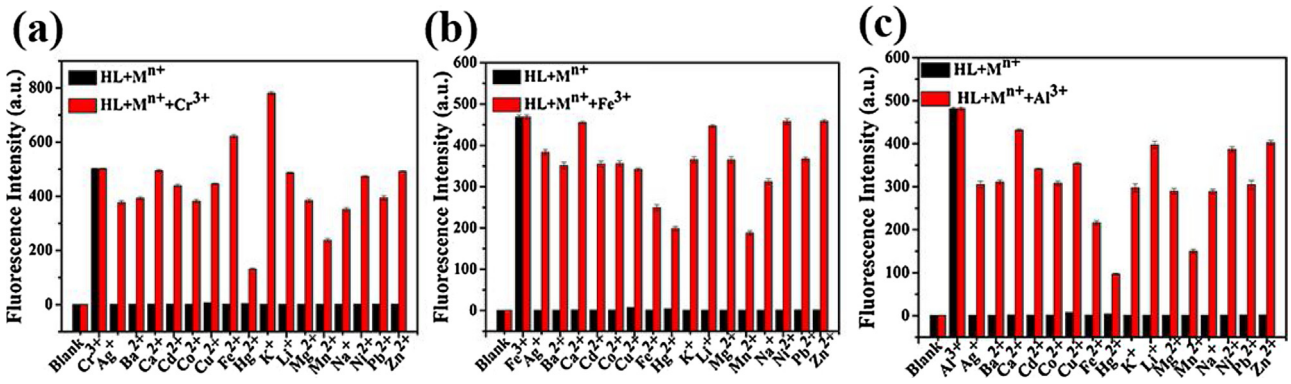

Fig. 5. Fluorescence response of **HL** (50 μM) upon addition of various metal cations (black bars: the fluorescence intensities of **HL** in the presence of other metal cations, red: the fluorescence intensities of **HL**-M^{n+} upon addition of *1 equiv. of* M^{3+}). (a): Cr^{3+}, (b): Fe^{3+}, and (c): Al^{3+}.

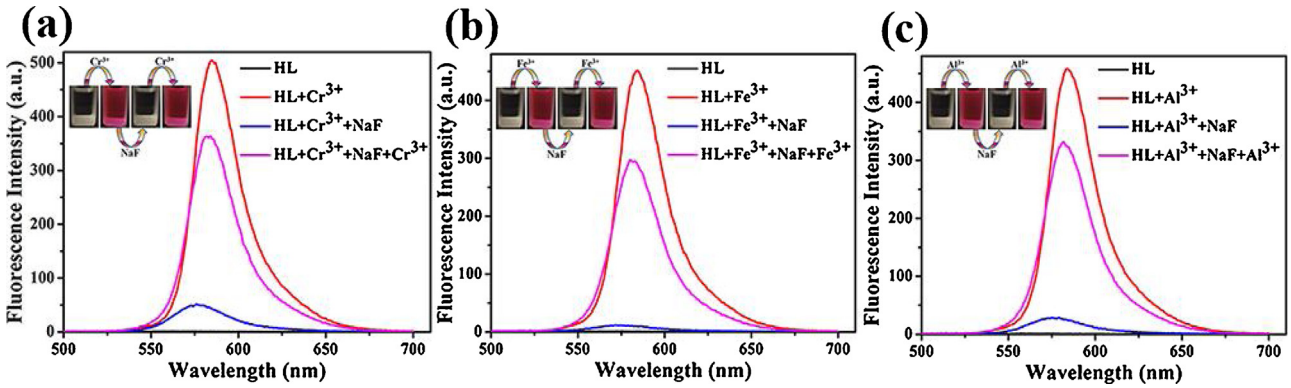

Fig. 6. Fluorescence spectral changes of **HL** (50 μM) after the sequential addition of M^{3+} and NaF (*2 equiv.*) in methanol. (a): Cr^{3+}, (b): Fe^{3+}, and (c): Al^{3+}. Inset: Images of fluorescence reversibility.

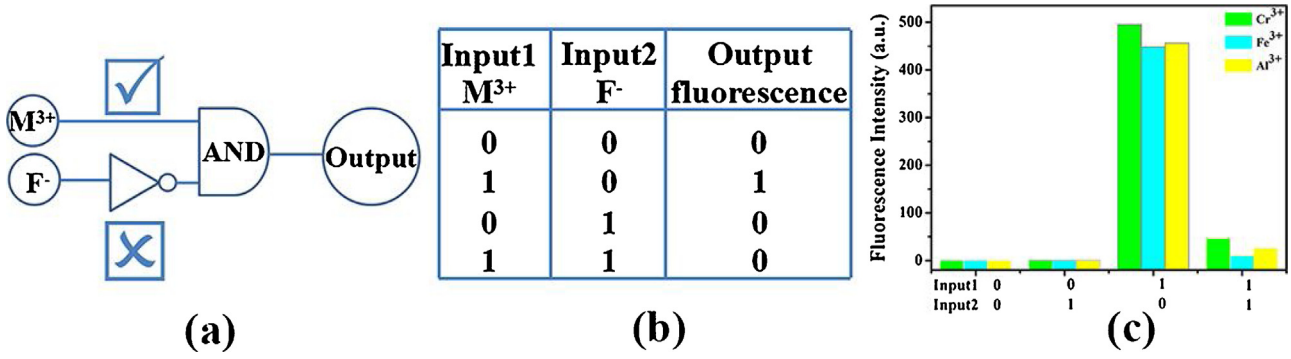

Input1 M^{3+}	Input2 F^-	Output fluorescence
0	0	0
1	0	1
0	1	0
1	1	0

Fig. 7. (a) The INHIBIT logic gate (integrated by combining a NOT, a YES, and an AND gate); (b) The corresponding truth table of this INHIBIT logic gate; (c) The output signals of fluorescence of this logic gate in the presence of different inputs.

HL was 0.5, which indicated that a possible 1:1 binding stoichiometry between **HL** and M^{3+}. To better confirm the binding mode of **HL** towards M^{3+}, the ESI mass spectrum of **HL** in the presence of M^{3+} were carried out (Fig. S15: Cr^{3+}, Fig. S16: Fe^{3+}, and Fig. S17: Al^{3+}). The *m*/*z* peak for **HL** in the presence of Cr^{3+} at 716.0940 corresponding to $[\mathbf{HL} + Cr^{3+} + Cl^- - H^+]^+$ and at 935.3586 corresponding to $[\mathbf{HL} + Cr^{3+} + 3DMF + Cl^- - H^+]^+$ (Fig. S15). The *m*/*z* peak for **HL** in the presence of Fe^{3+} at 685.1025 corresponding to $[\mathbf{HL} + Fe^{3+} - H^+]^{2+}$ and at 747.0802 corresponding to $[\mathbf{HL} + Fe^{3+} + NO_3^- - H^+]^+$ (Fig. S16). The *m*/*z* peak for **HL** in the presence of Al^{3+} at 820.1677 corresponding to $[\mathbf{HL} + Al^{3+} + 2DMF + H_2O - H^+]^{2+}$ and at 935.4058 corresponding to $[\mathbf{HL} + Al^{3+} + NO_3^- + DMF + 8H_2O - H^+]^+$ (Fig. S17). Thus, the mass spectrum data corroborated the 1:1 binding stoichiometry between **HL** and M^{3+}.

3.6. Proposed sensing mechanism of HL towards M^{3+}

To better understand the sensing mechanism of **HL** towards M^{3+}, the ^1H NMR titration experiments of **HL** in the presence of M^{3+} (Fe^{3+}) were carried out (Fig. S18). Upon addition of *1 equiv* M^{3+} (Fe^{3+}) to the DMSO-d_6 solution of **HL**, the proton signal of H_b (HNC=O) was broadened and shifted downfield from δ 10.17 ppm to δ

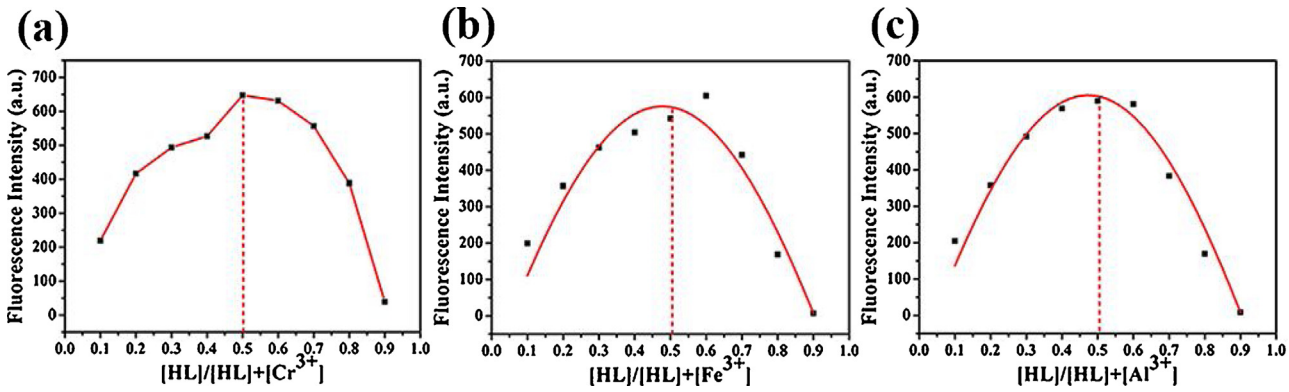

Fig. 8. Job's plot for determining the stoichiometry of **HL** and M^{3+} in methanol, the total concentration of **HL** and M^{3+} was kept 100 μM. (a): Cr^{3+}, (b): Fe^{3+}, and (c): Al^{3+}.

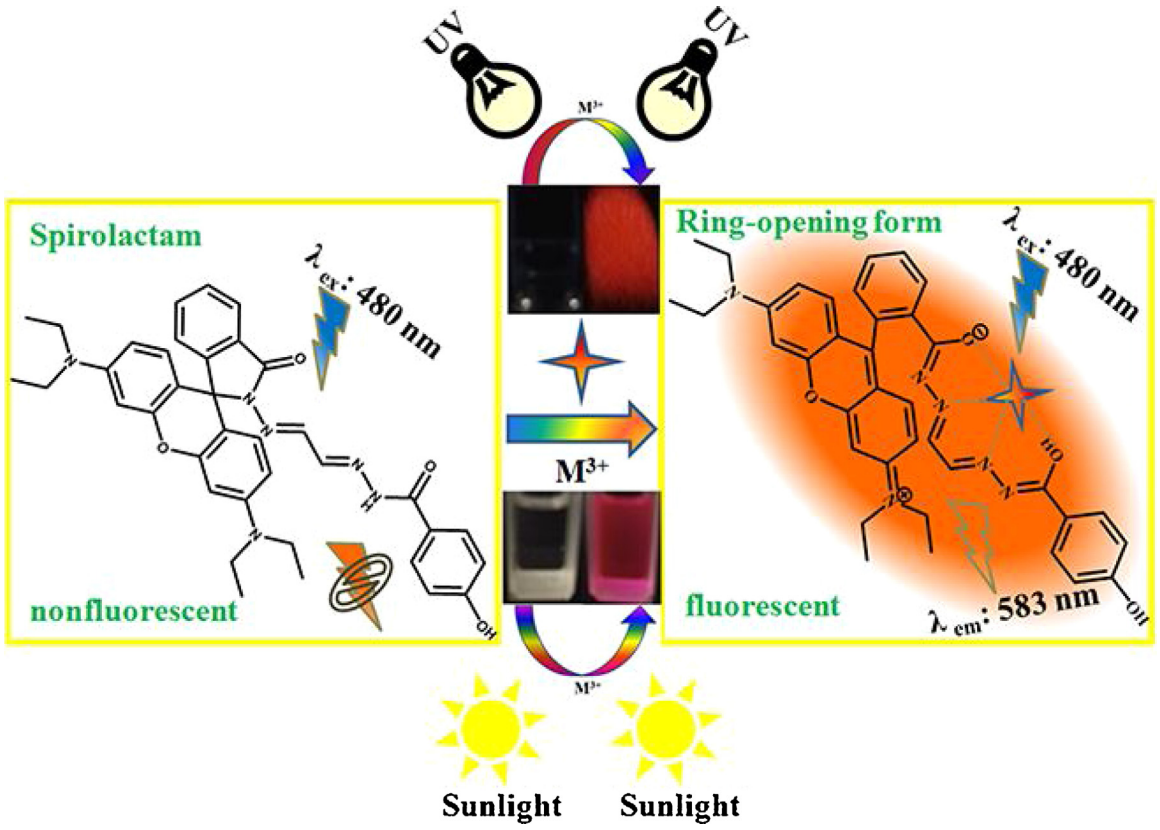

Scheme 2. The proposed sensing mechanism of **HL** towards M^{3+}.

10.21 ppm. Furthermore, the proton signals of the (CH=N) imines moieties were broadened and shifted downfield from δ 7.85 ppm and δ 7.98 ppm to δ 7.94 ppm and δ 8.03 ppm, respectively. The proton signal of H_c (-CH_3) was broadened and shifted up field from δ 1.09 ppm to δ 1.08 ppm and other proton signals on rhodamine B were also broadened and shifted up field. Additionally, the proton signal of H_a (-OH) was well retained with broadening and shifting downfield from δ 11.68 ppm to δ 11.70 ppm. These results indicated that the possible sensing mechanism is that M^{3+} binding with **HL** via nitrogen on the two imine moieties (CH=N), oxygen on the spirolactam, and oxygen on the amide group (HNC=O) induced the formation of ring opening of the rhodamine spirolactam (Scheme 2) [44–46].

4. Conclusion

In summary, we have designed and synthesized a new colorimetric "turn-on" fluorescent probe for M^{3+} (Cr^{3+}, Fe^{3+}, and Al^{3+}) based on rhodamine B derivative. The methanol solutions of **HL** in the presence of Cr^{3+}, Fe^{3+}, and Al^{3+} changed from colorless to pink accompanied with emitting orange-yellow fluorescence via the formation of ring-opened **HL**-M^{3+} complex. The Job's plot and

ESI-mass spectrometry analysis indicated that the 1:1 binding stoichiometry of **HL**-M^{3+}. Additionally, the binding of **HL** and M^{3+} was chemically reversible by the addition of fluorinion.

Acknowledgments

This work is supported by the National Natural Science Foundation of China (81171337). Gansu NSF (1308RJZA115).

Appendix A. Supplementary data

Supplementary data associated with this article can be found, in the online version, at https://doi.org/10.1016/j.jphotochem.2017.10.005.

References

[1] S. Goswami, S. Paul, A. Manna, RSC Adv. 3 (2013) 10639–10643.
[2] S. Goswami, A. Manna, S. Paul, A.K. Maity, P. Saha, C.K. Quah, H.K. Fun, RSC Adv. 4 (2014) 34572–34576.
[3] S. Goswami, A. Manna, S. Paul, K. Aich, A.K. Das, S. Chakraborty, Dalton Trans. 42 (2013) 8078–8085.
[4] S. Goswami, S. Paul, A. Manna, RSC Adv. 3 (2013) 25079–25085.
[5] D. Maity, T. Govindaraju, Inorg. Chem. 49 (2010) 7229–7231.
[6] D. Maity, T. Govindaraju, Chem. Commun. 46 (2010) 4499–4501.
[7] A. Sahana, A. Banerjee, S. Lohar, A. Banik, S.K. Mukhopadhyay, D.A. Safin, M.G. Babashkina, M. Bolte, Y. Garcia, D. Das, Dalton Trans. 42 (2013) 13311–13314.
[8] A. Banerjee, A. Sahana, S. Das, S. Lohar, B. Sarkar, S.K. Mukhopadhyay, A.K. Mukherjee, D. Das, Analyst 137 (2012) 2166–2175.
[9] L. Peng, Z.j. Zhou, X.Y. Wang, R.R. Wei, K. Li, Y. Xiang, A.J. Tong, Anal. Chim. Acta 829 (2014) 54–59.
[10] S. Paul, S. Goswami, A. Manna, Dalton Trans. 44 (2015) 11805–11810.
[11] B.B. Andrea, A.M. Costero, S. Gil, M. Parra, S. Juan, M.M. Ramon, S. Felix, Chem. Commun. 48 (2012) 3000–3002.
[12] X.J. Chen, X.Y. Shen, E. Guan, Y. Liu, A.J. Qin, J.Z. Sun, B.Z. Tang, Chem. Commun. 49 (2013) 1503–1505.
[13] Y.J. Jang, Y.H. Yeon, H.Y. Yang, J.Y. Noh, I.H. Hwang, C. Kim, Inorg. Chem. Commun. 33 (2013) 48–51.
[14] N.R. Chereddy, K. Saranraj, A.K. Barui, C.R. Patra, V.J. Rao, S. Thennarasu, RSC Adv. 4 (2014) 24324–24327.
[15] R. Alam, R. Bhowmick, A.S.M. Islam, A. Katarkar, K. Chaudhuri, M. Ali, New J. Chem. 41 (2017) 8359–8369.
[16] P. Mahato, S. Saha, E. Suresh, R.D. Liddo, P.P. Parnigotto, M.T. Conconi, M.K. Kesharwani, B. Ganguly, A. Das, Inorg. Chem. 51 (2012) 1769–1777.
[17] X.J. Wan, T.Q. Liu, H.Y. Liu, L.Q. Gu, Y.W. Yao, RSC Adv. 4 (2014) 29479–29484.
[18] S.Y. Tao, Y. Wei, C. Wang, Z.Q. Wang, P. Fan, D. Shi, B.J. Ding, J.S. Qiu, RSC Adv. 4 (2014) 46955–46961.
[19] S. von Haehling, S.D. Anker, Dtsch. Med. Wochenschr. 139 (2014) 841–844.
[20] S. Erdemir, O. Kocyigit, Talanta 158 (2016) 63–69.
[21] M.L. Presti, S.E. Sayed, R. Martinez-Manez, A.M. Costero, S. Gil, M. Parra, F. Sancenon, New J. Chem. 40 (2016) 9042–9045.
[22] N. Narayanaswamy, T. Govindaraju, Sens. Actuators B: Chem. 161 (2012) 304–310.
[23] S. Samanta, T. Ray, F. Haque, G. Das, J. Lumin. 171 (2016) 13–18.
[24] S. Samanta, S. Goswami, A. Ramesh, G. Das, J. Photochem. Photobiol. A 310 (2015) 45–51.
[25] T. Simon, M. Shellaiah, V. Srinivasadesikan, C.C. Lin, F.H. Ko, K.W. Sun, M.C. Lin, Sens. Actuators B: Chem. 231 (2016) 18–29.
[26] C. Marin-Hernandez, L.E. Santos-Figueroa, M.E. Moragues, M.M.M. Raposo, R. M.F. Batista, S.P.G. Costa, T. Pardo, R. Martinez-Manez, J. Org. Chem. 79 (2014) 10752–10761.
[27] S. Dey, S. Sarkar, D. Maity, P. Roy, Sens. Actuators B: Chem. 246 (2017) 518–534.
[28] S. Samanta, S. Goswami, A. Ramesh, G. Das, Sens. Actuators B 194 (2014) 120–126.
[29] T. Zhang, C.F. Chan, R.F. Lan, W.K. Wong, K.L. Wong, J. Chem. Eur. 20 (2014) 970–973.
[30] Q.Q. Li, M. Peng, H.Y. Li, C. Zhong, L. Zhang, X.H. Cheng, X.N. Peng, Q.Q. Wang, J. G. Qin, Z. Li, Org. Lett. 14 (2012) 2094–2097.
[31] X.Y. Lu, W.H. Zhu, Y.S. Xie, X. Li, Y. Gao, F.Y. Li, H. Tian, J. Chem. Eur. 16 (2010) 8355–8364.
[32] F.B. Yu, P. Li, G.Y. Li, G.J. Zhao, T.S. Chu, K.L. Han, J. Am. Chem. Soc. 133 (2011) 11030–11033.
[33] G. Sivaraman, T. Anand, D. Chellappa, Chem. Plus. Chem. 79 (2014) 1761–1766.
[34] G. Sivaraman, V. Sathiyaraja, D. Chellappa, J. Lumin. 145 (2014) 480–485.
[35] G. Sivaraman, B. Vidya, D. Chellappa, RSC Adv. 4 (2014) 30828–30831.
[36] G.L. Backes, D.M. Neumann, B.S. Jursic, Bioorg. Med. Chem. 22 (2014) 4629–4636.
[37] H. Peng, Y. Li, C. Jiang, R. Qi, R. Huang, C. Duan, T.S. Jadranka, Carbon 100 (2016) 386–394.
[38] X.H. Zhu, T.B. Zhao, Z. Nie, Z. Miao, Y. Liu, S.Z. Yao, Nanoscale 8 (2016) 2205–2211.
[39] C.R. Li, S.L. Li, Z.Y. Yang, Spectrochim. Acta A 174 (2017) 214–222.
[40] L.J. Tang, F.F. Li, M.H. Liu, R.J. Nandhakumar, Bull. Korean Chem. Soc. 32 (2011) 3400–3404.
[41] Z.D. Liu, H.J. Xu, L.Q. Sheng, S.S. Chen, D.Q. Huang, J. Liu, Spectrochim. Acta A 157 (2016) 6–10.
[42] (a) Z.Q. Li, Y. Zhou, K. Yin, Z. Yu, Y. Li, J. Ren, Dyes Pigm. 105 (2014) 7–11; (b) J.C. Qin, L. Fan, Z.Y. Yang, Sens. Actuators B: Chem. 228 (2016) 156–161; (c) X. Sun, Y.W. Wang, Y. Peng, Org. Lett. 14 (2012) 3420–3423.
[43] K. Boonkitpatarakul, J.F. Wang, N. Niamnont, B. Liu, L. Mcdonald, Y. Pang, M. Sukwattanasinitt, ACS Sens. 1 (2016) 144–150.
[44] A.J. Weerasinghe, F.A. Abebe, E. Sinn, Tetrahedron Lett. 52 (2011) 5648–5651.
[45] H. Yu, J.Y. Lee, S. Angupillai, S. Wang, S.H. Feng, S. Matsumoto, Y.A. Son, Acta Part A 151 (2015) 48–55.
[46] Q.P. Hu, Y.L. Liu, Z.Q. Li, R.Z. Wen, Y. Gao, Y.L. Bei, Q.Z. Zhu, Tetrahedron Lett. 55 (2014) 4912–4916.